NANO LETTERS

2008
Vol. 8, No. 7
1916-1922

Elucidating the Role of Surface Hydrolysis in Preparing Organosilane Nanostructures via Particle Lithography

Jie-Ren Li and Jayne C. Garno*

Department of Chemistry and the Center for BioModular Multi-Scale Systems, Louisiana State University, Baton Rouge, Louisiana 70803

Received February 28, 2008; Revised Manuscript Received June 4, 2008

ABSTRACT

A new method of particle lithography is described for preparing rings or nanoporous films of organosilanes. Millions of exquisitely uniform and precisely spaced nanostructures with designed surface chemistry can be rapidly produced using vapor deposition through mesoparticle masks. Nanoscopic amounts of water are essential for initiating surface hydrosilation. Thus, the key step for preparing covalently bonded nanostructures of organosilanes is to control drying parameters to spatially direct the placement of water on surfaces.

The great promise of nanotechnology relies on capabilities to organize nanomaterials on surfaces to create assemblies with designed surface properties.[1–3] Currently, it is a challenge to control surface chemistry at the nanoscale for preparing functional systems for electronic,[4] optoelectronic,[5] biological,[6] or sensing[7] applications. Nanoscale lithography methods will facilitate development of well-defined molecular architectures that can be applied for devices such as protein chips[8,9] or molecular junctions.[10–13] We have developed a new method for nanopatterning organosilanes using vapor deposition and particle lithography. Using colloidal masks produced by particle lithography, the placement of nanoscopic residues of water can be well-controlled to spatially direct the sites for hydrolysis of organosilanes. Silane nanopatterns produced by particle lithography exhibit highly reproducible geometries and enable nanoscale control of the surface chemistry of nanostructures.

Self-assembled monolayers (SAMs) furnish a model platform for engineering surfaces at the molecular level.[14,15] Due to the ease of preparation and well-ordered structures, SAMs of *n*-alkanethiols[16] and *n*-alkylsilanes[17] have been used for surface modification, protein adsorption, and molecular device fabrication.[18,19] Films of organosilanes resist oxidative and thermal degradation. The alkyl chain length and terminal moieties of silane SAMs can be tailored to suit experimental requirements. The covalent nature of siloxane bonds within silane SAMs provides stability and durability for nanostructures. Silane SAMs form siloxane bonds that anchor to the surface and also cross-link to form interconnections with adjacent molecules. There is a competition for the formation of Si−O bridges to adjacent molecules, connections to the substrate or production of silanols, Si-OH. The amount of cross-linking depends on various conditions of sample preparation such as the nature of the substrate and immersion solvent and temperature.[20] The terminal moieties of silanes present various functional groups on surfaces, such as methyl, amine, glycol, etc., which offers extensive possibilities for generating SAM nanostructures with designed selectivity and reactivity. Substrates that have been used to prepare alkylsilane SAMs include silicon oxide, aluminum oxide, germanium oxide, quartz, glass, and mica.[14] For substrates that contain relatively few hydroxyl groups, such as mica(0001), prehydrolysis of alkylsilanes[21] or water vapor exposure to the surfaces[22] has been used to effect hydrosilation.

Organosilane monolayers can be prepared from solution[23–25] or vapor phase[26–28] to form densely packed monolayers. The molecular density and film quality of silane SAMs depends on parameters such as the amount of water, the temperature, the choice of immersion media, adsorption time, the type of organosilane molecule chosen, and the chemical nature of the surface.[20] In a densely packed silane SAM, the alkyl chains would be oriented nearly perpendicular to the substrate with a tilt angle of 0−5° (Figure 1).[14] A broad range of experimental conditions have been used to prepare organosilane layers and consequently the molecular organization, packing, and surface properties reported for the resulting structures have been inconsistent.[20] The self-assembly of octadecyltrichlorosilane (OTS) has been studied extensively using ellipsometry,[23,25,28–32] X-ray reflectometry,[25,33,34] infrared spectroscopies,[31,32,35] grazing incidence X-ray diffraction (GIXD),[34] neutron reflectivity,[36] X-ray photoelectron spectroscopy,[30] and atomic force microscopy

* Corresponding author. Phone: 225-578-8942. Fax: 225-578-3458. E-mail: jgarno@lsu.edu.

10.1021/nl0806062 CCC: $40.75
Published on Web 06/19/2008

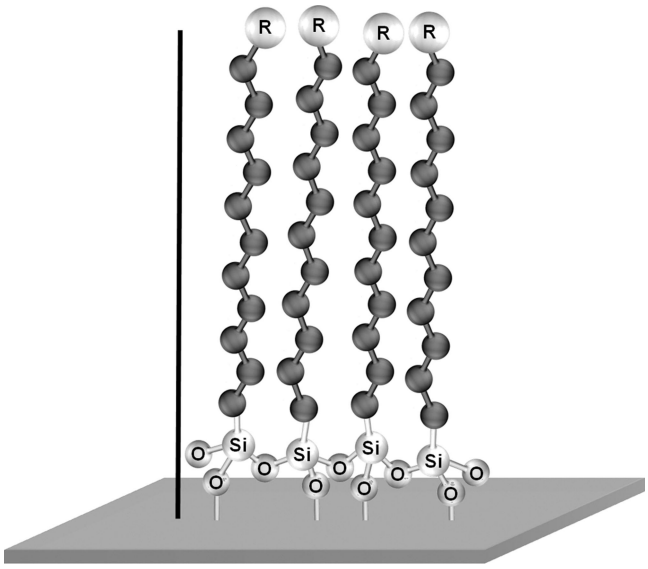

Figure 1. General structure of organosilane self-assembled monolayers.

Scheme 1. Generalized Mechanism for the Hydrolysis of Trichlorosilanes on Surfaces[17]

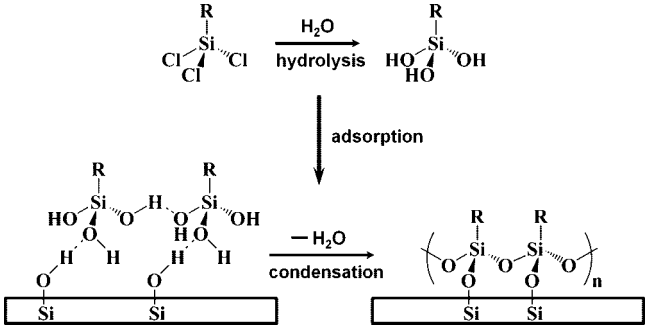

(AFM).[25,29,30] In these reports, the thickness values ranged from to 2.25 to 2.81 nm for a SAM of OTS. The alkyl chains adopt an all-trans configuration with tilt angle values reported that ranged from 0 to 17°. The range of measured values can be attributed to differences in surface coverage and diverse methods of sample preparation for OTS. In particular, the amount of water present in solvents is a critical parameter which affects formation of an organosilane monolayer.[37–39] The role of water in forming silane SAMs was reported by Sagiv, who observed that water adsorbed on a glass surface is necessary to initiate hydrolysis of OTS.[17] If too much water is present, polymerization of silanes to form polysiloxanes can occur in solution, rather than forming films on surfaces.[29,38,40]

The general steps of the hydrolysis of trichlorosilanes to form SAMs on surfaces are outlined in Scheme 1.[17] Alkylsilane molecules react with a trace amount of water to bond covalently to surfaces. Silanol molecules produced by hydrolysis adsorb to surface reactive sites and undergo a condensation reaction with free hydroxyl groups. Each hydrolyzed silane molecule can form siloxane bonds to anchor to the surface and also connect to neighboring molecules to form a network of Si−O−Si bridges. The chlorosilane groups can also convert to silanols or form additional linkages to the surface.[28] Trace amounts of water are essential to form densely packed silane monolayers and the quality of SAMs depends on the degree of hydration of the substrate.[40–42] To form organosilane SAMs, it can be difficult to control trace amounts of water to consistently produce high quality films with continuous well-packed domains of high density. Even ambient humidity can adversely affect the reproducibility of forming alkylsilane SAMs. In the absence of water, organosilane SAMs form incomplete monolayers and are generally of poor quality.

A range of lithographic approaches have been applied for patterning organosilane monolayers. Photolithography with silane SAMs is accomplished by UV irradiation through photomasks.[43] Silane monolayers in exposed regions can be selectively removed via a photocleavage mechanism; the uncovered areas of the surface can then be used for further modification with different SAMs. Photolithography can also be applied to change the chemistry of surface head groups by UV-activated photochemistry.[44] The resolution of SAM patterns produced by photolithography is limited by diffraction of light sources and by the dimensions of the photomasks. Electron beam lithography can overcome the diffraction limitation of light sources to generate smaller patterns with dimensions less than 100 nm.[26,45,46] However, e-beam lithography requires considerable training and expensive instrumentation. Approaches using soft lithography, such as microcontact printing with polydimethylsilane (PDMS) stamps have been applied successfully for patterning silane monolayers.[47,48] The dimensions of silane patterns are limited to the size of the PDMS templates, typically at the micrometer scale. Also, one must choose solvents which do not dissolve PDMS for ink solutions. Approaches using scanning probe lithography (SPL) including Dip-Pen nanolithography,[49,50] nanoshaving,[51,52] bias-induced lithography,[53] and constructive nanolithography[54–56] have also been applied to write nanopatterns of silane SAMs. These methods provide exquisite nanoscale resolution and enable us to subsequently visualize the surface morphology with great detail. However, the patterns are fabricated one at a time, by slow serial writing processes which are not easily scaled to the high throughput and reproducibility needed for device manufacture.

Particle lithography or nanosphere lithography uses the arrangement of spherical particles to produce ordered arrays of regular nanostructures on surfaces.[57,58] Monodisperse spheres self-assemble on flat surfaces into periodic structures with designed dimensions and interparticle spacing, which can then be used as structural templates or masks to guide the deposition of metals,[59–61] inorganic materials,[62–64] polymers,[65–67] catalysts,[68] and proteins.[69–71]

Molecules such as *n*-alkanethiol SAMs have been patterned using particle lithography. Colloidal masks were applied in a method of edge-spreading lithography (ESL) to produce nanosized rings on gold or silver surfaces.[72,73] For ESL, a PDMS stamp was inked with alkanethiols and placed on a film of silica microspheres that had been dried on gold or silver surfaces. Alkanethiol molecules were delivered from the surface of the PDMS stamp through the mesoparticle layer to the metal substrate to form circular patterns

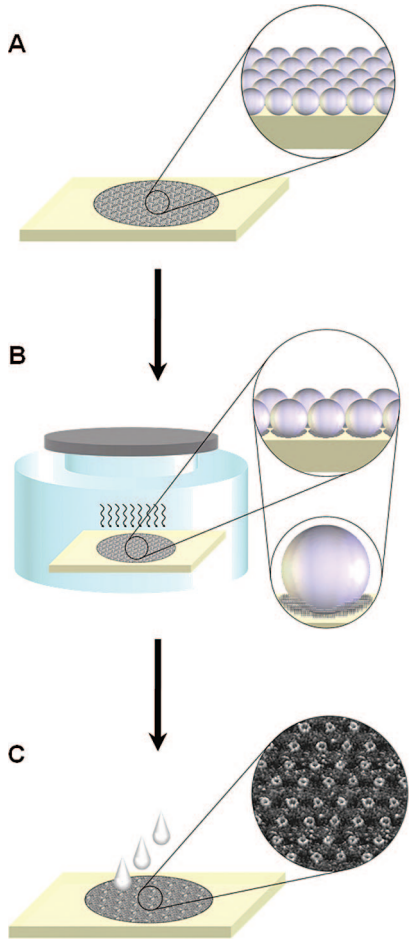

Figure 2. Steps of the new procedure for particle lithography. (A) A dried film of monodisperse latex spheres provides a mask for vapor deposition. (B) A vapor of alkylsilanes is generated by heating a sealed vessel. (C) The latex mask is rinsed away to reveal silane nanopatterns.

surrounding the areas masked by silica spheres. A method of contact angle lithography was developed to produce pore-shaped structures of silane SAMs using silica particles as masks.[74] For this approach, silicon substrates coated with a mask of silica colloids were immersed in a toluene solution containing silanes. Silane molecules self-assembled in the interstitial areas of the surface between silica spheres. Immersion of colloidal masks can be a problem because of the buoyancy of the mesoparticles in various liquids. Silica and latex spheres rapidly detach from surfaces during immersion steps of particle lithography.

We introduce a new approach for patterning silane SAMs that combines particle lithography with vapor deposition to generate nanopatterns. The procedural steps are outlined in Figure 2. First, solutions containing monodisperse latex particles (Duke Scientific, Palo Alto, CA) are deposited on ultraflat surfaces. Ruby muscovite mica (Sand J and Trading Co., NY) and double-sided polished silicon(111) doped with boron (Virginia Semiconductor Inc., Fredericksburg, VA) were used for our investigations. Size-sorted monodisperse latex mesospheres (Duke Scientific, Palo Alto, CA) were initially washed with deionized water by centrifugation. The spheres form a pellet at the bottom of a microcentrifuge tube, which can then be resuspended in deionized water. Next, a drop of the mesoparticle suspension is placed on a substrate and dried at room temperature. As water evaporates during drying, capillary forces pull the mesospheres together to form organized crystalline layers on flat surfaces (Figure 2A).[75] The dried film of mesospheres provides a mask for evaporation. The dried masks of colloidal silica spheres are then placed into a sealed vessel containing a few drops of the alkylsilanes to be patterned. The molecules used for preparing nanopatterns, octadecyltrichlorosilane (OTS), 2-[methoxy-(polyethyleneoxy)propyl]trichlorosilane (PEG-silane), and *N*-(6-aminopropyl)aminomethyltrimethoxysilane (AAPTMS) were purchased from Gelest (Morrisville, PA). To generate a vapor, the reaction vessel was placed in an oven at 70 to 80 °C under ambient pressure (Figure 2B). During vapor deposition, organosilanes adsorb through self-assembly onto uncovered interstitial areas of the surface between latex spheres. The area of contact between the substrate and the base of the spheres is effectively masked to produce patterns with circular geometries. In the final step, the latex masks are removed completely by sonication and rinsing in ethanol (Pharmco, Aaper, TX). The silanes bond covalently to the substrates and are not displaced from the surface by the rinsing step. Depending on the drying parameters, arrays of rings or pore-shaped silane nanostructures are generated (Figure 2C).

Silane nanostructures were imaged with a model 5500 atomic force microscope (AFM) (Agilent Technologies, Tempe, AZ) using acoustic AC-mode imaging, which operates the cantilever in the intermittent contact regime. For AC-mode AFM, the oscillation of the AFM tip is driven by applying an AC voltage to a piezoactuator. Rectangular silicon nitride cantilevers with force constants ranging from 21 to 98 N m^{-1} and a resonance frequency of 165 kHz were purchased from Nanosensors (Lady's Island, SC) and used for acoustic AC-mode imaging. Images were processed using Gwyddion (version 1.12) open source software, which is freely available on the Internet and supported by the Czech Metrology Institute.[76]

The surface coverage and geometry of OTS nanostructures on mica exhibit distinct differences when the latex masks were dried under different conditions (Figure 3). For latex masks that were dried briefly (20−60 min), arrays of OTS nanopatterns with pore-shaped morphologies were produced as shown in the AFM topography images of Figure 3A,B. A film of OTS with circular areas of uncovered substrate is revealed where the latex spheres were displaced. The thickness of the OTS layer is relatively even across the surface, uniformly covering the areas between the cavities where latex particles were displaced. The thickness of the film measures 2.2 ± 0.3 nm, referencing the uncovered areas of the substrate as a baseline (Figure 3C). Measurements of the periodicity of the nanopatterns were calculated by averaging the distances between the centers of the pores for at least 200 nanostructures from several representative areas of the surface. The average periodicity of OTS pores for the examples in Figure 3A,B measured 309 ± 8 nm and matches well with the expected diameter of the latex mesospheres

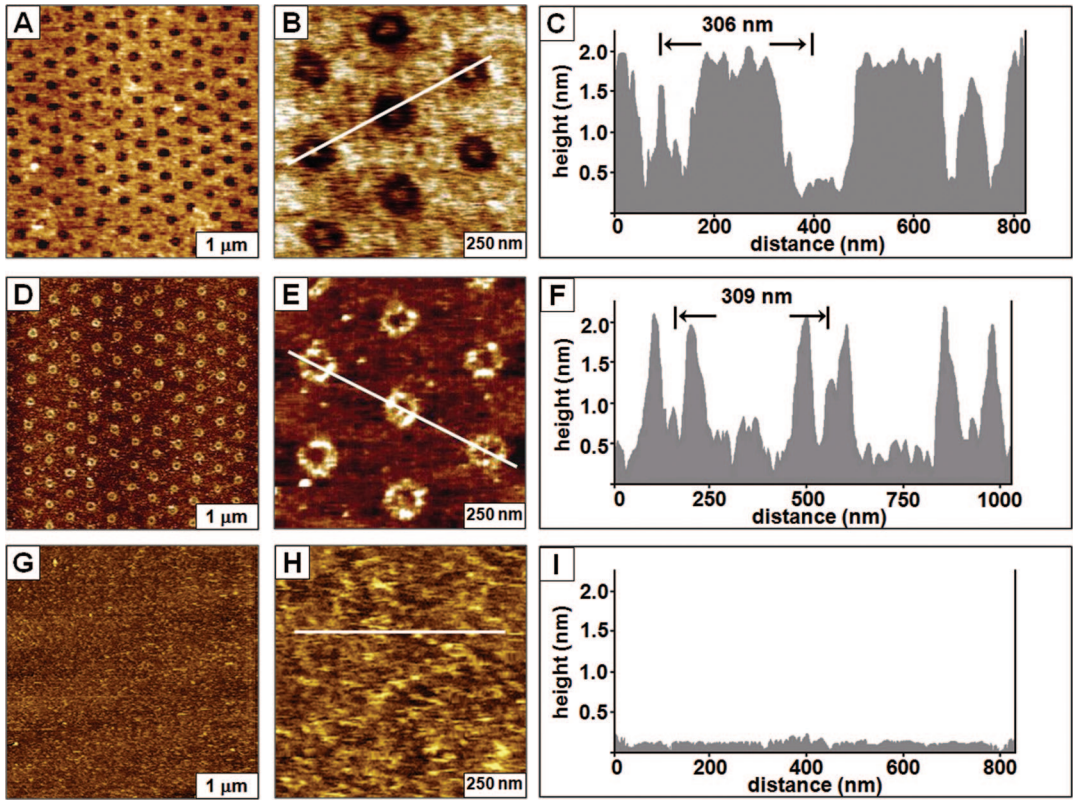

Figure 3. Differences in nanopattern morphologies with various drying conditions. (A) Octadecyltrichlorosilane nanopatterns produced on mica(0001) using a 300 nm latex mask that was dried briefly, 20 min; (B) zoom-in view; (C) corresponding cursor profile for panel B. (D) ring-shaped nanopatterns fabricated using 300 nm latex masks dried under ambient conditions for 12 h. (E) close-up view of hexagonal arrangement of rings; (F) cursor profile for panel E. (G, H) patterns did not form on mica surfaces when latex masks were dried in an oven; (I) cursor profile for the line in panel H.

(299 ± 6 nm). Small islands of OTS formed within the pores of the nanostructured film as shown in Figure 3B. If the latex spheres do not make tight conformal contact with the substrate then water can be trapped underneath the spheres. With the vapor deposition process, OTS molecules bind at the site of water residues. Such islands were not observed for spheres that were smaller than 300 nm or when using polished silicon wafers as substrates.

Ring structures of OTS can be generated by drying the latex masks for 12 h as displayed in Figure 3D,E. Aligned rows and columns of ring patterns that form a hexagonal arrangement are generated with precisely replicated geometries. For masks that have been dried for several hours, AFM images reveal that OTS only binds in areas near the base of the latex spheres to form ring structures. The height of the rings measures 2.1 ± 0.4 nm (Figure 3F). The periodicity of the OTS rings for the sample of Figure 3D,E averages 311 ± 6 nm, which corresponds to the diameter of the latex spheres.

When masks of 300 nm latex were fully dried in an oven (95 °C, 24 h), OTS nanostructures were not generated after exposure to silane vapors as viewed in Figure 3G,H. The cursor profile (Figure 3I) provides further evidence that OTS structures did not form. A few loose adsorbates are present on the surface that affects tip adhesion; however there is no evidence of defined periodic structures present in AFM topographs. With oven-dried latex templates, the topographic images of Figure 3G,H do not exhibit a surface morphology that is representative of covalently bound OTS on mica(0001).[51,77]

For organosilanes to bind to substrates, nanoscopic amounts of water are needed to initiate surface hydrolysis. After vapor deposition, AFM images clearly display surface areas with residues of water as viewed for silane nanostructures in Figure 3. These results demonstrate that the amount of water on surfaces is a critical parameter for controlling the sites for hydrolysis of OTS. For latex masks that have been dried briefly, water is distributed homogeneously throughout areas of the surface to enable molecular self-assembly of a thin film covering interstitial areas between mesoparticles. As vapors are introduced, OTS assembles surrounding the base of the masks and also binds to any uncovered areas of the surface between latex spheres. Only the areas masked by the latex spheres are protected from silane adsorption. When colloidal masks are dried under ambient conditions (25 °C, relative humidity ~60%) for longer intervals, (12−24 h), most of the water evaporates from the surface. Only tiny residues of water persist to form a circular meniscus in areas surrounding the base of latex spheres. When the partially dried latex masks are exposed to OTS vapor, hydrolysis occurs only where water is present: at the base of spheres. For latex masks that were oven-dried (95 °C, 24 h), nanostructures of OTS did not form in the absence of water.

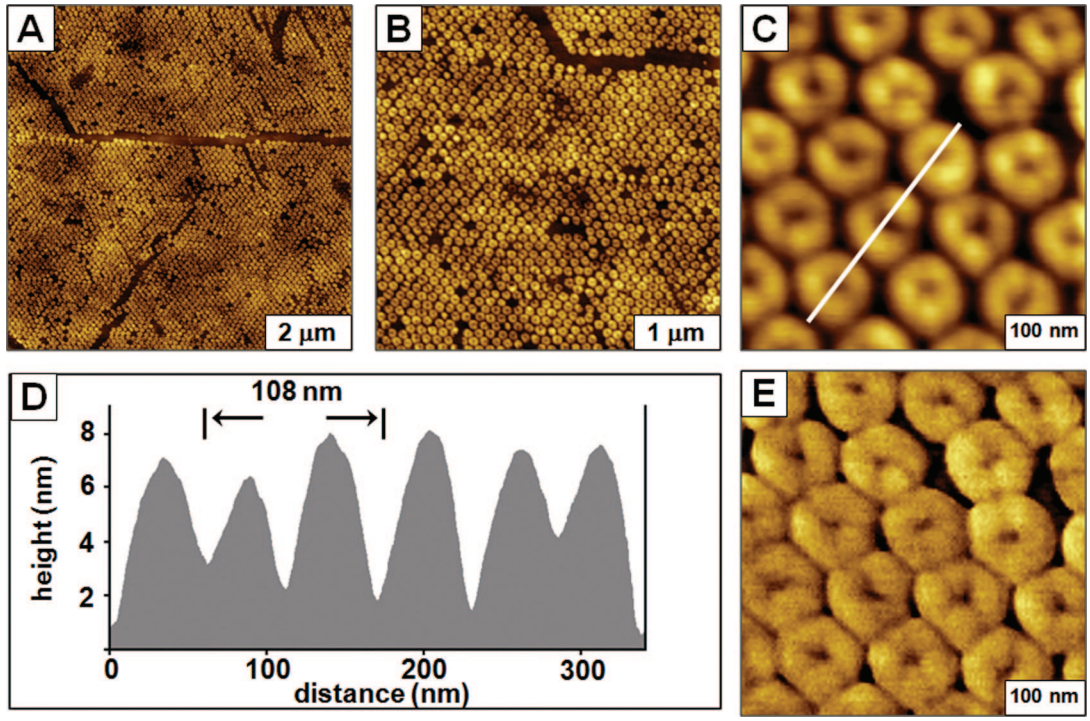

Figure 4. Rings of PEG-terminated silane SAMs prepared with 100 nm latex masks. (A) Long range order and packing of ring structures; (B) close-up view of nanopatterns; (C) zoom-in of 100 nm rings; (D) cursor profile for the line in panel C; (E) phase image of panel C.

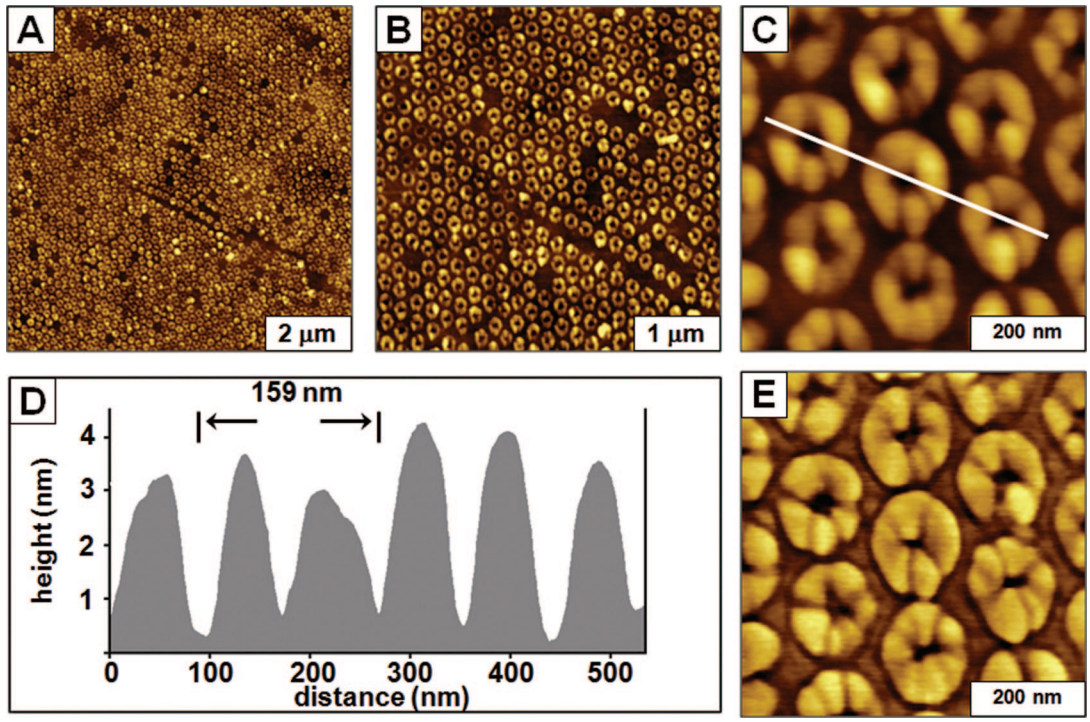

Figure 5. Amine-terminated silane nanopatterns produced using 150 nm latex masks. (A) Broad view of ring-shaped nanopatterns; (B) zoom view of silane nanostructures; (C) hexagonal arrangement of rings; (D) cursor plot for panel C; (E) phase image of panel C.

Particle lithography was also applied successfully for organosilanes with different functional headgroups, such as 2-[methoxy(polyethyleneoxy)propyl]trichlorosilane (PEG-silane). Poly-(ethylene glycol) silanes are used as coatings for microfluidic devices, microarrays, and biosensors to reduce nonspecific adsorption of biomolecules or cells onto surfaces while maintaining a hydrophilic, biocompatible surface.[78,79] A generic approach used for surface-bound protein assays is to pattern PEG silanes to prevent nonspecific binding of proteins.[80] An example of periodic arrays of PEG-silane rings that were fabricated on silicon substrates using 100 nm latex particles is shown in Figure 4. The latex masks were dried for 24 h in ambient air, which produced individual ring-shaped nanostructures throughout areas of the surface.

The long-range order and organization of PEG-silane rings is apparent in the successive zoom-in views (Figure 4A,B,C) with only a few defects produced by missing particles. Other researchers have developed approaches to minimize the density of defects for particle lithography by using fabrication steps with convective assembly[81] or Langmuir−Blodgett troughs.[82] The phase image of Figure 4E displays differences in elastic response between PEG rings and uncovered areas of the substrate. The uniform contrast of the surfaces of the rings indicates that the chemistry is homogeneous. The height of the PEG-silane rings measures 8.3 ± 0.8 nm with an average periodicity of 107 ± 5 nm (Figure 4D) which corresponds well with the expected diameter of the latex masks (97 ± 3 nm). The width of the PEG-silane rings measures 67 ± 8 nm with an inner pore diameter of 31 ± 4 nm. The width of gap in between adjacent rings measures 18 ± 5 nm. There are 19 PEG-silane rings within the 0.5 × 0.5 μm^2 frame of Figure 4C, whereas the larger 8 × 8 μm^2 area of Figure 4A has 4870 ring patterns. This yields an estimated ring density of 7.6×10^9 nanostructures per 1 × 1 cm^2.

Amine-terminated silane nanostructures can also be produced by particle lithography combined with vapor deposition. Periodic arrays of rings of *N*-(6-aminopropyl)aminomethyltrimethoxysilane (AAPTMS) were prepared on silicon surfaces using 150 nm latex masks that had been dried in air for 24 h (Figure 5). Within the 8 × 8 μm^2 topography image of Figure 5A there are 2310 rings, evidencing the high-throughput capabilities of particle lithography. The ring-shaped geometry of AAPTMS nanopatterns is highly consistent, shown by successive zoom-in views of Figure 5A,B,C. The average width of the AAPTMS rings formed by 150 nm latex spheres measures 117 ± 7 nm, and the size of pores within the rings is 56 ± 9 nm. The average periodicity of 155 ± 8 nm measured for the arrays of AAPTMS nanopatterns corresponds closely to the dimensions of the latex masks (151 ± 4 nm). The zoom-in topography (Figure 5C) and corresponding phase image (Figure 5E) reveal that the rings do not touch neighboring patterns. Phase images distinguish differences in surface chemistry and elastic response. The AAPTMS rings have a uniform surface composition with a brighter contrast relative to the uncovered areas of silicon between the nanopatterns. The height of the AAPTMS nanopatterns measures 3.7 ± 0.5 nm (Figure 5D), which is taller than the expected dimensions for a single layer of AAPTMS (∼2.0 nm).

Particle lithography is a practical approach for fabricating nanopatterns with designed surface chemistry. Nanopatterns of organosilane SAMs can be generated reproducibly by combining particle lithography with chemical vapor deposition. The placement of water adsorbed to surfaces is a critical factor for determining the sites of hydrosilation to form silane nanostructures via vapor deposition. A general observation is that the surface morphologies were highly consistent and reproducible for a specific drying condition and particle diameter. Once the experimental conditions are optimized, dozens of samples prepared with the selected conditions exhibit identical nanoscale morphologies. The geometry of alkylsilane nanopatterns is determined by the drying conditions of the latex masks. The drying parameters provide a means to control the distribution and placement of nanoscopic residues of water. Silanes bind only to the areas of the surface containing trace amounts of water, since water is essential for hydrosilation. By adjusting the time interval for drying the masks, nanoscopic residues of water on surfaces can be retained near the bases of spherical masks to spatially direct the sites for hydrosilation. The surface density, as well as the size and periodicity of the nanostructures can be selected by choosing various latex diameters. In future work, patterns of organosilane SAMs will be used as a foundation to attach metals, organic molecules and nanomaterials in well-defined surface architectures.

Acknowledgment. The authors gratefully acknowledge support from the NSF-sponsored Center for BioModular Multi-Scale Systems at LSU, the ACS Petroleum Research Fund, PRF G43352-G5 and the State of Louisiana Board of Regents, RCS subprogram, LEQSF(2006-09)-RD-A-04. J.-R.L. thanks Pfizer for a graduate fellowship in analytical chemistry. We also thank Z. M. LeJeune, K. L. Lusker, and S. Verberne-Sutton for helpful discussion.

References

(1) Barth, J. V.; Costantini, G.; Kern, K. *Nature* **2005**, *437* (7059), 671–679.
(2) Rosi, N. L.; Mirkin, C. A. *Chem. Rev.* **2005**, *105* (4), 1547–1562.
(3) Woodson, M.; Liu, J. *Phys. Chem. Chem. Phys.* **2007**, *9* (2), 207–225.
(4) Gimzewski, J. K.; Joachim, C. *Science* **1999**, *283* (5408), 1683–1688.
(5) Link, S.; El-Sayed, M. A. *J. Phys. Chem. B* **1999**, *103* (40), 8410–8426.
(6) Cui, Y.; Wei, Q. Q.; Park, H. K.; Lieber, C. M. *Science* **2001**, *293* (5533), 1289–1292.
(7) Medintz, I. L.; Uyeda, H. T.; Goldman, E. R.; Mattoussi, H. *Nat. Mater.* **2005**, *4* (6), 435–446.
(8) Wadu-Mesthrige, K.; Xu, S.; Amro, N. A.; Liu, G. Y. *Langmuir* **1999**, *15* (25), 8580–8583.
(9) Hyun, J.; Ahn, S. J.; Lee, W. K.; Chilkoti, A.; Zauscher, S. *Nano Lett.* **2002**, *2* (11), 1203–1207.
(10) Reed, M. A.; Zhou, C.; Muller, C. J.; Burgin, T. P.; Tour, J. M. *Science* **1997**, *278* (5336), 252–254.
(11) Joachim, C.; Gimzewski, J. K.; Aviram, A. *Nature* **2000**, *408* (6812), 541–548.
(12) Carroll, R. L.; Gorman, C. B. *Angew. Chem., Int. Ed.* **2002**, *41* (23), 4379–4400.
(13) Nitzan, A.; Ratner, M. A. *Science* **2003**, *300* (5624), 1384–1389.
(14) Ulman, A. *Chem. Rev.* **1996**, *96* (4), 1533–1554.
(15) Schreiber, F. *Prog. Surf. Sci.* **2000**, *65* (5−8), 151–256.
(16) Nuzzo, R. G.; Allara, D. L. *J. Am. Chem. Soc.* **1983**, *105* (13), 4481–4483.
(17) Sagiv, J. *J. Am. Chem. Soc.* **1980**, *102* (1), 92–98.
(18) Love, J. C.; Estroff, L. A.; Kriebel, J. K.; Nuzzo, R. G.; Whitesides, G. M. *Chem. Rev.* **2005**, *105* (4), 1103–1169.
(19) Onclin, S.; Ravoo, B. J.; Reinhoudt, D. N. *Angew. Chem., Int. Ed.* **2005**, *44* (39), 6282–6304.
(20) Wen, K.; Maoz, R.; Cohen, H.; Sagiv, J.; Gibaud, A.; Desert, A.; Ocko, B. M. *ACS Nano* **2008**, *2* (3), 579–599.
(21) Kessel, C. R.; Granick, S. *Langmuir* **1991**, *7* (3), 532–538.
(22) Schwartz, D. K.; Steinberg, S.; Israelachvili, J.; Zasadzinski, J. A. N. *Phys. Rev. Lett.* **1992**, *69* (23), 3354–3357.
(23) Wasserman, S. R.; Tao, Y.-T.; Whitesides, G. M. *Langmuir* **1989**, *5*, 1074–1087.
(24) Maoz, R.; Sagiv, J. *Langmuir* **1987**, *3* (6), 1034–1044.
(25) Rozlosnik, N.; Gerstenberg, M. C.; Larsen, N. B. *Langmuir* **2003**, *19* (4), 1182–1188.
(26) Pallandre, A.; Glinel, K.; Jonas, A. M.; Nysten, B. *Nano Lett.* **2004**, *4* (2), 365–371.

(27) Hoffmann, P. W.; Stelzle, M.; Rabolt, J. F. *Langmuir* **1997**, *13* (7), 1877–1880.
(28) Fadeev, A. Y.; McCarthy, T. J. *Langmuir* **2000**, *16*, 7268–7274.
(29) Vallant, T.; Brunner, H.; Mayer, U.; Hoffmann, H.; Leitner, T.; Resch, R.; Friedbacher, G. *J. Phys. Chem. B.* **1998**, *102*, 7190–7197.
(30) Jeon, N. L.; Finnie, K.; Branshaw, K.; Nuzzo, R. G. *Langmuir* **1997**, (1997), 3382–3391.
(31) Allara, D. L.; Parikh, A. N.; Rondelez, F. *Langmuir* **1995**, *11*, 2357–5360.
(32) Parikh, A. N.; Allara, D. L.; Azouz, I.; Rondelez, F. *J. Phys. Chem.* **1994**, *98*, 7577–7590.
(33) Richter, A. G.; Durbin, M. K.; Yu, C.-J.; Dutta, P. *Langmuir* **1998**, *14*, 5980–5983.
(34) Kojio, K.; Takahara, A.; Omote, K.; Kajiyama, T. *Langmuir* **2000**, *16*, 3932–3936.
(35) Hoffmann, H.; Mayer, U.; Krischanitz, A. *Langmuir* **1995**, *11*, 1304–1312.
(36) Fragneto, G.; Lu, J. R.; McDermott, D. C.; Thomas, R. K.; Rennie, A. R.; Gallagher, P. D.; Satija, S. K. *Langmuir* **1996**, *12*, 477–486.
(37) Tripp, C. P.; Hair, M. L. *Langmuir* **1992**, *8*, 1120–1126.
(38) Carson, G. A.; Granick, S. *J. Mater. Res.* **1990**, *5*, 1745–1751.
(39) Krasnoslobodtsev, A. V.; Smirnov, S. N. *Langmuir* **2002**, *18* (8), 3181–3184.
(40) Tripp, C. P.; Hair, M. L. *Langmuir* **1992**, *8* (4), 1120–1126.
(41) Angst, D. L.; Simmons, G. W. *Langmuir* **1991**, *7* (10), 2236–2242.
(42) Le Grange, J. D.; Markham, J. L.; Kurkjian, C. R. *Langmuir* **1993**, *9* (7), 1749–1753.
(43) Dulcey, C. S.; Georger, J. H.; Krauthamer, V.; Stenger, D. A.; Fare, T. L.; Calvert, J. M. *Science* **1991**, *252* (5005), 551–554.
(44) Brandow, S. L.; Chen, M. S.; Aggarwal, R.; Dulcey, C. S.; Calvert, J. M.; Dressick, W. J. *Langmuir* **1999**, *15* (16), 5429–5432.
(45) Lercel, M. J.; Redinbo, G. F.; Pardo, F. D.; Rooks, M.; Tiberio, R. C.; Simpson, P.; Craighead, H. G.; Sheen, C. W.; Parikh, A. N.; Allara, D. L. *J. Vac. Sci. Technol., B* **1994**, *12* (6), 3663–3667.
(46) Lercel, M. J.; Craighead, H. G.; Parikh, A. N.; Seshadri, K.; Allara, D. L. *Appl. Phys. Lett.* **1996**, *68* (11), 1504–1506.
(47) Xia, Y. N.; Mrksich, M.; Kim, E.; Whitesides, G. M. *J. Am. Chem. Soc.* **1995**, *117* (37), 9576–9577.
(48) Wang, D. W.; Thomas, S. G.; Wang, K. L.; Xia, Y. N.; Whitesides, G. M. *Appl. Phys. Lett.* **1997**, *70* (12), 1593–1595.
(49) Ivanisevic, A.; Mirkin, C. A. *J. Am. Chem. Soc.* **2001**, *123* (32), 7887–7889.
(50) Jung, H.; Kulkarni, R.; Collier, C. P. *J. Am. Chem. Soc.* **2003**, *125* (40), 12096–12097.
(51) Jourdan, J. S.; Cruchon-Dupeyrat, S. J.; Huan, Y.; Kuo, P. K.; Liu, G. Y. *Langmuir* **1999**, *15* (19), 6495–6504.
(52) Headrick, J. E.; Armstrong, M.; Cratty, J.; Hammond, S.; Sheriff, B. A.; Berrie, C. L. *Langmuir* **2005**, *21* (9), 4117–4122.
(53) Gu, J. H.; Yam, C. M.; Li, S.; Cai, C. Z. *J. Am. Chem. Soc.* **2004**, *126* (26), 8098–8099.
(54) Maoz, R.; Frydman, E.; Cohen, S. R.; Sagiv, J. *Adv. Mater.* **2000**, *12* (6), 424–429.
(55) Maoz, R.; Frydman, E.; Cohen, S. R.; Sagiv, J. *Adv. Mater.* **2000**, *12* (10), 725–731.
(56) Hoeppener, S.; Maoz, R.; Sagiv, J. *Nano Lett.* **2003**, *3* (6), 761–767.
(57) Haynes, C. L.; Van Duyne, R. P. *J. Phys. Chem. B* **2001**, *105* (24), 5599–5611.
(58) Xia, Y. N.; Gates, B.; Yin, Y. D.; Lu, Y. *Adv. Mater.* **2000**, *12* (10), 693–713.
(59) Tessier, P.; Velev, O. D.; Kalambur, A. T.; Lenhoff, A. M.; Rabolt, J. F.; Kaler, E. W. *Adv. Mater.* **2001**, *13* (6), 396–400.
(60) Haynes, C. L.; Van Duyne, R. P. *Nano Lett.* **2003**, *3* (7), 939–943.
(61) Chen, Z.; Zhan, P.; Wang, Z. L.; Zhang, J. H.; Zhang, W. Y.; Ming, N. B.; Chan, C. T.; Sheng, P. *Adv. Mater.* **2004**, *16* (5), 417–422.
(62) Jiang, P.; Bertone, J. F.; Colvin, V. L. *Science* **2001**, *291* (5503), 453–457.
(63) Meng, Q. B.; Fu, C. H.; Einaga, Y.; Gu, Z. Z.; Fujishima, A.; Sato, O. *Chem. Mater.* **2002**, *14* (1), 83–88.
(64) Kuo, C. W.; Shiu, J. Y.; Chen, P. L.; Somorjai, G. A. *J. Phys. Chem. B* **2003**, *107* (37), 9950–9953.
(65) Jiang, P.; Hwang, K. S.; Mittleman, D. M.; Bertone, J. F.; Colvin, V. L. *J. Am. Chem. Soc.* **1999**, *121* (50), 11630–11637.
(66) Briseno, A. L.; Han, S. B.; Rauda, I. E.; Zhou, F. M.; Toh, C. S.; Nemanick, E. J.; Lewis, N. S. *Langmuir* **2004**, *20* (1), 219–226.
(67) Marquez, M.; Patel, K.; Carswell, A. D. W.; Schmidtke, D. W.; Grady, B. P. *Langmuir* **2006**, *22* (19), 8010–8016.
(68) Gustavsson, M.; Fredriksson, H.; Kasemo, B.; Jusys, Z.; Kaiser, J.; Jun, C.; Behm, R. J. *J. Electroanal. Chem.* **2004**, *568* (1−2), 371–377.
(69) Garno, J. C.; Amro, N. A.; Wadu-Mesthrige, K.; Liu, G. Y. *Langmuir* **2002**, *18* (21), 8186–8192.
(70) Li, J. R.; Henry, G. C.; Garno, J. C. *Analyst* **2006**, *131* (2), 244–250.
(71) Cai, Y. G.; Ocko, B. M. *Langmuir* **2005**, *21* (20), 9274–9279.
(72) McLellan, J. M.; Geissler, M.; Xia, Y. N. *J. Am. Chem. Soc.* **2004**, *126* (35), 10830–10831.
(73) Geissler, M.; McLellan, J. M.; Chen, J. Y.; Xia, Y. N. *Angew. Chem., Int. Ed.* **2005**, *44* (23), 3596–3600.
(74) Bae, C.; Shin, H. J.; Moon, J.; Sung, M. M. *Chem. Mater.* **2006**, *18* (5), 1085–1088.
(75) Denkov, N. D.; Velev, O. D.; Kralchevsky, P. A.; Ivanov, I. B.; Yoshimura, H.; Nagayama, K. *Langmuir* **1992**, *8* (12), 3183–3190.
(76) Gwyddion. http://gwyddion.net/, Czech Metrology Institute: 2007.
(77) Xiao, X. D.; Liu, G. Y.; Charych, D. H.; Salmeron, M. *Langmuir* **1995**, *11* (5), 1600–1604.
(78) Kingshott, P.; Griesser, H. J. *Curr. Opin. Solid State Mater. Sci.* **1999**, *4* (4), 403–412.
(79) Herrwerth, S.; Eck, W.; Reinhardt, S.; Grunze, M. *J. Am. Chem. Soc.* **2003**, *125* (31), 9359–9366.
(80) Choi, I.; Kang, S. K.; Lee, J.; Kim, Y.; Yi, J. *Biomaterials* **2006**, *27* (26), 4655–4660.
(81) Prevo, B. G.; Velev, O. D. *Langmuir* **2004**, *20* (6), 2099–2107.
(82) Marquez, M.; Grady, B. P. *Langmuir* **2004**, *20* (25), 10998–11004.

NL0806062